Polymer 290 (2024) 126526

Contents lists available at ScienceDirect

Polymer

journal homepage: www.elsevier.com/locate/polymer

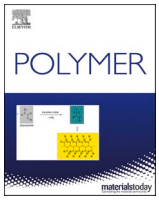

Photopolymerization-induced phase separation kinetics explored by intermittent irradiation

Lauren Zakrzewski [a], Chang Y. Ryu [a], Chulsung Bae [a], Catalin R. Picu [b,*]

[a] Department of Chemistry and Chemical Biology, Rensselaer Polytechnic Institute, Troy, NY, 12180, USA
[b] Department of Mechanical, Aerospace and Nuclear Engineering, Rensselaer Polytechnic Institute, Troy, NY, 12180, USA

ARTICLE INFO

Keywords:
Photo-PIPS
Phase separation
Thermosets
Kinetics

ABSTRACT

In this work, we explore the kinetics of the photopolymerization-induced phase separation (photo-PIPS) process and the interplay of mechanisms controlling the development of the microstructure in a photosensitive resin comprised of pentaerythritol tetraacrylate (PETA) and 2-ethylhexyl methacrylate (2-EHMA) monomers with polypropylene glycol (PPG, M_n = 4000 g/mol) linear polymer additive and diphenyl(2,4,6-trimethylbenzoyl) phosphine oxide (TPO) photoinitiator. We control the kinetics of photopolymerization by interrupting the irradiation at various stages of the process and varying the light intensity. Evolution of the microstructure is monitored by transmittance testing and scanning electron microscopy (SEM) inspection of fractured surfaces that are exposed to methanol for the purpose of removing the phase-separated PPG content. The evolution of the network is monitored by real-time Fourier-transform infrared (FTIR) spectroscopy during irradiation and intermittent probing after the cessation of irradiation. Three mechanisms controlling the evolution of the microstructure are identified: phase separation, photoinitiator consumption, and microstructural refinement. Phase separation begins immediately after the onset of network development and leads to a rapid reduction of transmittance due to the formation of PPG-rich subdomains. Microstructural refinement takes place at later stages leading to a reduction of these subdomains, a gradual increase of the PPG concentration within subdomains and an associated increase of transmittance. TPO consumption takes place during irradiation and accounts, to a smaller extent, for the recovery of the transmittance. Interrupting the irradiation allows generation of materials with various degrees of conversion and sizes of phase-separated subdomains, which provides a new way to control material properties.

1. Introduction

It has been established that introducing heterogeneity to thermosets may lead to enhanced optical and mechanical properties. In terms of unique optical properties, systems have been developed with phase-separated liquid crystal domains which offer holographic characteristics [1–5]. Regarding mechanical properties, addition of elastomeric particles improves the toughness and offers a commercial solution to the intrinsic, and undesirable, brittleness of thermosets [6–14]. Likewise, nanoscale solutions based on various alterations of the network architecture have been considered. The addition of nanoparticles [13,15–20], the use of block copolymers [21–24], and the use of polymer blends [25–31] are alternative ways to adjust the microstructure and have shown to improve the toughness of thermoset materials to various degrees. However, all these methods are not free of drawbacks. For instance, while nanoparticles are able to disperse quite well in a monomer resin up to high concentrations, they are quite expensive and their use is quite limited [15–20]. For polymer blends, the lack of easily miscible polymer systems poses a significant challenge [25–32]. For block copolymers, synthetic conditions to obtain the desired polymer chain architecture are tedious and restricted [21–24,32]. A somewhat less restrictive method for producing thermosets with complex microstructures is the use of polymerization-induced phase separation (PIPS) [11,33–50]. PIPS yields these microstructures by forming phase-separated subdomains during polymer network development. PIPS can be performed through various methods of polymerization including cationic [51], anionic [52], and radical photopolymerization (photo-PIPS) [32,53–69]. In this work, we report our study of kinetics and the mechanisms which govern network development in radical photo-PIPS.

* Corresponding author.
E-mail address: picuc@rpi.edu (C.R. Picu).

https://doi.org/10.1016/j.polymer.2023.126526
Received 5 October 2023; Received in revised form 17 November 2023; Accepted 20 November 2023
Available online 23 November 2023

Photo-PIPS proceeds initially with a homogeneous, liquid multicomponent monomer resin consisting of monomer(s), photoinitiator, and polymer additive(s) or nanoparticles which are immiscible with the developing network upon light irradiation and photopolymerization [32,33,53–64]. During photopolymerization, the immiscible species creates its own phase-separated subdomains and develops a heterogeneous material. The PIPS process is driven by thermodynamic driving forces described by the Flory-Huggins equation,

$$\frac{\Delta G_{mix}}{nRT} = \frac{\varphi_A \, ln \, \varphi_A}{N_A} + \frac{\varphi_B ln \, \varphi_B}{N_B} + \chi \varphi_A \varphi_B \quad (1)$$

where N_x and φ_x are the degree of polymerization and volume fraction of each component, respectively, and n is the total number of molecules [11,33,53,70–72]. The first two terms are entropic, while the third one describes the enthalpy of mixing. Polymerization of one component in a multicomponent resin produces changes in entropy, while particular chemistries of the polymer chains define χ. Larger χ corresponds to larger immiscibility between components. Molecular diffusion controls the kinetics and ultimately the extent of phase separation possible in the PIPS process. In resins containing reactive oligomers and linear polymer chains of the phase-separating agent, as used in this work, the diffusion of oligomers is faster than that of the polymer additive. From this, the kinetics of the phase separation process is seen to be controlled by the initial formation of the network. Systems reaching complete phase separation attain thermodynamic equilibrium. In all other cases, phase separation is incomplete, thus the structure is determined by the rate of photopolymerization.

While PIPS is known to be more convenient for producing a heterogeneous polymeric material than the use of block copolymers and polymer blends, it still has its limitations. Specifically, the following three phenomena are known to be difficult to control: i) internal stress state, ii) polymer microstructure (type of phase separation, bicontinuous structures, subdomain sizes, etc.), and iii) interfacial properties between phases [11,73]. Residual stress in a polymeric network depends on the extent of shrinkage as well as the number of defects present in the resulting network [74]. Fine tuning of the polymerization kinetics could promote more uniformly crosslinked networks [73,74]. The network morphology can be adjusted by varying the chemistries of the resin components, such as chain length of polymer additives or size of nanoparticles, and concentrations of the polymer additives or nanoparticles [30–32,57]. The use of polymer additives with a small difference in χ to the developing network leads to a low driving force for phase separation, slow kinetics, and potentially a different phase-separated morphology (nucleation and growth vs spinodal decomposition) [32,53,56,60,61,71]. The interfacial properties between the two separate phases could be adjusted, for example, through the addition of block copolymers [11].

The present work focuses on the kinetics of the photo-PIPS process and the mechanisms that govern the developing microstructure. We control the kinetics by varying the light intensity and by stopping irradiation at various stages of the process to observe the evolution of the structure by intermittent probing. We show that phase separation starts with the onset of network formation and leads to the rapid reduction of light transmittance. This initial stage is followed by microstructural refinement (i.e., reduction of the size of the phase-separated subdomains), which leads to enhanced homogeneity and gradual increase of transmittance. Intermittent irradiation allows for control of the phase-separated subdomain size. The strategies explored provide a way to develop photo-curable materials with tunable microstructures and material properties.

2. Materials and methods

2.1. Materials

The resins used in this work are comprised of a photoinitiator and two acrylate monomers with one and four polymerizable sites, respectively. One of the resins also contains a polymer additive. Pentaerythritol tetraacrylate (PETA, M_n = 352 g/mol), a four-arm acrylate monomer, is purchased from TCI Chemicals and used as the first monomeric component. 2-Ethylhexyl methacrylate (2-EHMA, M_n = 198 g/mol), a methacrylate diluent and single-arm methacrylate monomer, is purchased from Sigma-Aldrich and is used as the second monomeric component. Diphenyl(2,4,6-trimethylbenzoyl) phosphine oxide (TPO, M_n = 348 g/mol), is used as the photoinitiator and polypropylene glycol (PPG, M_n = 4000 g/mol) is used as the polymer additive, both also being supplied by Sigma-Aldrich. Fig. 1 illustrates the chemical structures of these components. The monomeric ratio is 3:1 by weight of acrylate monomer to methacrylate diluent (PETA:2-EHMA 75:25 by wt%). TPO photoinitiator in powder form is added to this mixture in 0.5 wt% and stirred with gentle heating at ~60 °C to create a homogeneous photo-curable neat resin. To develop the phase-separating resin, 15 wt% of PPG polymer additive is added to the neat resin and stirred at ~60 °C to fully dissolve within the photo-curable resin. The two resins investigated in this system are denoted as "PE neat resin" and "PE 4000," where the "PE" stands for the two monomeric components contained (**P**ETA:2-**E**HMA), and the number denotes the molecular weight of the polymer additive.

2.2. Custom-built phase separation detection apparatus

To visualize the extent of phase separation in the PPG-containing photo-curable resin, a custom-built light transmission apparatus is used to measure the light transmittance. The apparatus consists of a S120VC Photodiode Power Sensor (wavelength of absorption = 200–1100 nm, ThorLabs), a LX500 OmniCure portable LED UV-lamp, and a sample compartment. This apparatus was previously described in our previous works and additional information is provided in Section 1 of the Supplementary Information (SI) [75,76].

Samples are prepared by adding liquid resin to a glass slide prepped with spacers to allow for uniform thickness and sandwiched with a coverslip. Transmittance tests are performed using a sample thickness b = 100 μm. Thicknesses are measured via profilometry upon complete photopolymerization (see Section 2.3). Samples are exposed for different durations at constant light intensity using a wavelength of 405 nm (wavelength range at half peak height of the lamp spectrum is 398–412 nm, while the detector is tuned to a wavelength of 405 nm exactly). If phase separation occurs, a corresponding rapid reduction in transmittance would be seen due to light scattering. In cases of no phase separation, transmittance slightly increases over time due to TPO photoinitiator consumption, following the reactive Beer-Lambert Law. Various durations of light exposure are used to monitor the phase separation process and network development. Continuous exposure times of t_c = 5, 10, 45, 60, and 900 s are applied in separate experiments, at a light intensity of 4.9 mW/cm^2, while transmittance data collection is performed every 30 ms. To study the process after irradiation has ceased, the system is irradiated continuously for a duration t_c (5, 10, or 45 s), after which the light is turned off and probing is performed with light pulses of the same wavelength and of 0.4 s duration. These probing points are equally separated in time on a 1.5x log scale, up to a total monitoring time of 900 s. The probing duration of 0.4 s is chosen so that the light detector has enough time to acquire an accurate transmittance reading while also limiting further photopolymerization of the resin. This same experiment is also run using a lower light intensity of 1.3 mW/cm^2. In this case, t_c = 15, 30, and 105 s, with probing occurring in the same manner.

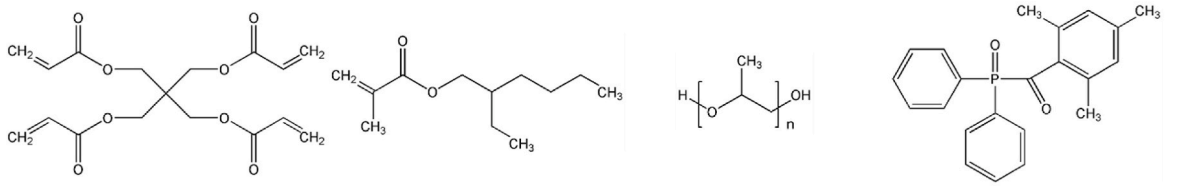

Pentaerythritol tetraacrylate (PETA) | 2-ethylhexyl methacrylate (2-EHMA) | Polypropylene glycol (PPG) | Diphenyl(2,4,6-trimethylbenzoyl)phosphine oxide (TPO)

Fig. 1. Monomer resin components and their corresponding chemical structures.

2.3. Material characterization

Monomer conversion, induction time of photopolymerization, and the rate of photopolymerization of both photo-curable resins are determined through real-time FTIR spectroscopy analysis using a Thermo-Scientific Nicolet iS50 FT-IR equipped with an attenuated total reflectance (ATR) attachment (PIKE Technologies GladiATR). Real-time FTIR experiments are performed within the wavenumber range of 4000 to 400 cm^{-1} during photopolymerization. Like the transmittance tests, a LX500 OmniCure portable LED UV-lamp of wavelength 405 nm is used for photopolymerization. A custom-made 3D-printed part is used to hold the LED UV-lamp and cover the top of the ATR stage. This allows for the light dose supplied to the resin sample to be maintained throughout the experiment. Light intensities of 1.3 and 4.9 mW/cm^2 are used for the real-time FTIR measurement. Film thicknesses are maintained at 100 μm by using Scotch tape as a spacer. Liquid resin is added to the ATR crystal, a coverslip is placed, and the 3D-printed part holding the LED UV-lamp is then placed on top, with the lamp aligned with the ATR crystal. The resin is then continuously irradiated for 900 s while collecting FTIR data every 0.08 s. Probed systems previously described in Section 2.2 are also tested using real-time FTIR where the system is irradiated for a certain duration of time and then probed intermittently for 0.4 s until 900 s is reached. This experiment is only performed for the 4.9 mW/cm^2 light intensity. The durations of exposure prior to probing are 5, 10, and 45 s.

The monomer conversion data is obtained by first acquiring the peak height ratios of two peaks within the Omnic software. The absorbance of the (meth)acrylate carbonyl –C═O stretching peak at 1724 cm^{-1} is used as an internal reference. The absorbance of the (meth)acrylate alkene –C═C stretching peak at 1627 cm^{-1} is compared to the internal reference as this C═C bond present in the acrylate and methacrylate monomers is consumed during photopolymerization. The ratio of absorbance, A, of these peaks is used to calculate a conversion spectrum. The monomer conversion, C, is computed as:

$$C(t)\ [\%] = (1 - A(t) / A(0)) \times 100 \quad (2)$$

The rate of photopolymerization is estimated by taking the derivative of the monomer conversion. The induction time of photopolymerization is identified as the time at which monomer conversion begins to increase from 0 %.

Scanning electron microscopy (SEM), is used to examine the polymer film morphologies of the phase-separating resin, PE 4000. A Versa 3-D Focused Ion Beam - Scanning Electron Microscope (FIB-SEM) by Thermo Fisher Scientific is used. Polymer films are prepared by first adding a layer of liquid monomer resin to a glass slide with spacers to allow for uniform thickness of 100 μm, similar to the light transmittance experiment preparations outlined in Section 2.2. This glass slide is then sealed with a coverslip and inserted into the custom-built light transmission apparatus. The sample is then irradiated at a light intensity of 4.9 mW/cm^2 for the durations indicated in Section 2.2 for both the probed and non-probed systems. Following irradiation, films are gently separated from the glass slide and coverslip using a razor, being mindful of the side which was exposed to light. These films are then wiped dry to remove any residual monomer resin. Next, the films are placed in a bath of liquid nitrogen for approximately 30 s, removed, and fractured from a shallow notch incised with a razor. The fractured films are washed for 2 min in methanol to remove the PPG polymer additive and any leftover monomer resin. The removal of PPG enables the visualization of the subdomains induced by phase separation of PPG. A piece of double-sided carbon tape is placed on a SEM sample stub, on which the films are placed. The films are placed so that their cross sections are facing upwards and are flush to the edge of the tape. The films are then sputter coated with a layer of Au/Pd for ~1 min. Secondary electron images are obtained using an accelerating voltage of 5.0 kV, a working distance of 10 mm, and a beam current of 5.9 pA. MATLAB is used to calculate the coefficient of variation (CV) of the roughness of the respective polymer cross-sections (CV is defined as the standard deviation divided by the mean of the image intensity).

Profilometry using a Dektak 8 Contact Profilometer from Veeco Instruments Inc. is used to obtain the polymer film thickness for the PE neat and PE 4000 resins after light transmittance experiments for all the continuous doses of irradiation considered at 4.9 mW/cm^2 light intensity (5, 10, 45, 60, and 900 s of continuous exposure). Scan parameters include a scanning distance of 4,000 μm, a duration of 60 s, a stylus force of 5 mg, and a measurement range of 2,620 kÅ. Samples were tested starting from the edge of the 5 mm diameter circular film, tracing across the center.

3. Results and discussion

3.1. Effect of cessation of irradiation on monomer conversion and transmittance

Phase separation is monitored in this work (and in our previous work [75]) using transmittance, T. A typical T(t) curve for the phase-separating PE 4000 resin subjected to continuous irradiation for 900 s is shown in Fig. 2a and labeled "continuous." The curve exhibits a sharp reduction of T beyond the induction time of phase separation, followed by recovery and a plateau which emerges once the system attains thermodynamic equilibrium [11,70,72,75]. We conjecture that the variation of transmittance is associated with the following mechanisms:

Mechanism 1: Phase separation. Transmittance is reduced as the system phase separates and scatters light. This scattering is caused by a difference in refractive index of the resin and the PPG subdomains that emerge by phase separation, as discussed in Section 2 of the SI. This is also supported by the work of Szczepanski et al. [32] where a reduction in light transmission was seen in cases of large concentrations and large molecular weights of PMMA polymer additive. In their works, the development of phase-separated PMMA subdomains in a TEGDMA network formed during photopolymerization causes reduction in light transmission due to differences in RI of the two phases [32].

Mechanism 2: Photoinitiator consumption. TPO absorbs light in the spectral range used for irradiation and probing (see Section 3 of the SI). Hence, as the concentration of TPO is reduced during photopolymerization, transmittance increases accordingly following the reactive Beer-Lambert Law.

Mechanism 3: Variation of subdomain size. Continued network

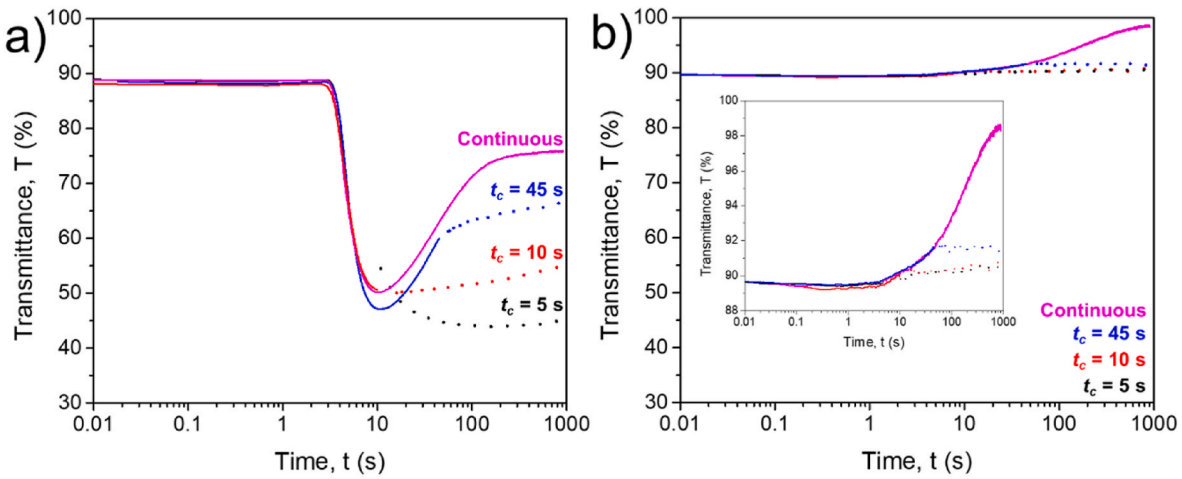

Fig. 2. The intermittent irradiation transmittance curves for various exposure times for the (a) PE 4000 and (b) PE neat resins. All systems are irradiated with 4.9 mW/cm^2 light intensity.

crosslinking leads to the shrinkage/fragmentation of the phase-separated subdomains, ultimately causing microstructural refinement as illustrated in Fig. 3. A corresponding increase in transmittance results due to enhanced homogeneity of the material.

We note that higher UV intensities (larger than 15 mW/cm^2) cause PPG crystallization in the PPG 4000 system, but this is not observed at the intensity used in this work. Therefore, crystallization makes no contribution to the transmittance in the present experiments. The following discussion provides evidence and evaluates the relative contributions of these mechanisms to microstructural evolution.

To eliminate mechanism 2 in our phase-separating system, we stop irradiation after time t_c of continuous irradiation and probe the structural evolution by intermittent irradiation. TPO consumption and the formation of new radicals is ceased at t_c. We select t_c = 5, 10, and 45 s in separate experiments and show the corresponding T(t) curves in Fig. 2a.

T(t) behaves differently at times $t > t_c$ for the three values of the cutoff time, t_c, for the PE 4000 resin (Fig. 2a). The case of t_c= 5 s follows the decreasing branch of T(t) of the continuously irradiated system and exhibits a continuous decrease of T(t) after the cessation of irradiation, as indicated by the probing points. This portrays that phase separation continues to develop even without light exposure due to the presence of radicals formed at $t < t_c$. In other words, mechanism 1 supersedes mechanism 3 at this stage in network development. The case of t_c= 10 s corresponds to the minimum of the T(t) curve obtained by continuous irradiation. A slight increasing trend is seen in T(t) for $t > t_c$, which indicates that mechanisms 1 and 3 compensate each other. Lastly, the case of t_c= 45 s corresponds to a stage of the continuously irradiated system beyond the minimum of T(t). In this case, T(t) increases steadily for $t > t_c$, which indicates that mechanism 3 dominates.

In the PE neat resin system however, there is little change in transmittance at any of the three cutoff points (t_c = 5, 10, or 45 s), as shown in Fig. 2b. In these cases, all mechanisms are inactive for $t > t_c$. In addition, network shrinkage (which is a component of mechanism 3) takes place upon crosslinking both with and without phase separation. Since in the PE neat resin case T(t) has an insignificant change for $t > t_c$, we conclude that network shrinkage alone has a weak effect on T(t). This is likely due to the fact that the neat resin is already a much more homogeneous network than the PE 4000 system. Therefore, when further crosslinking occurs due to activated radicals in the PE neat resin, little increase in homogeneity is achieved. In the phase-separated network of PE 4000, continued network crosslinking leads not only to network shrinkage, but also to the refinement of the PPG subdomains, as discussed further in Section 3.2, which turns out to have a greater effect on transmittance.

To demonstrate that the network continues to evolve even after the light is turned off, real-time FTIR experiments were performed using the same intermittent irradiation conditions as for the transmittance tests for both resin systems. Fig. 4a shows the monomer conversion of the PE neat resin for the continuous irradiation case and all t_c cases considered. The conversion increases monotonically in all cases, including in the intermittent irradiation systems for $t > t_c$. However, the maximum

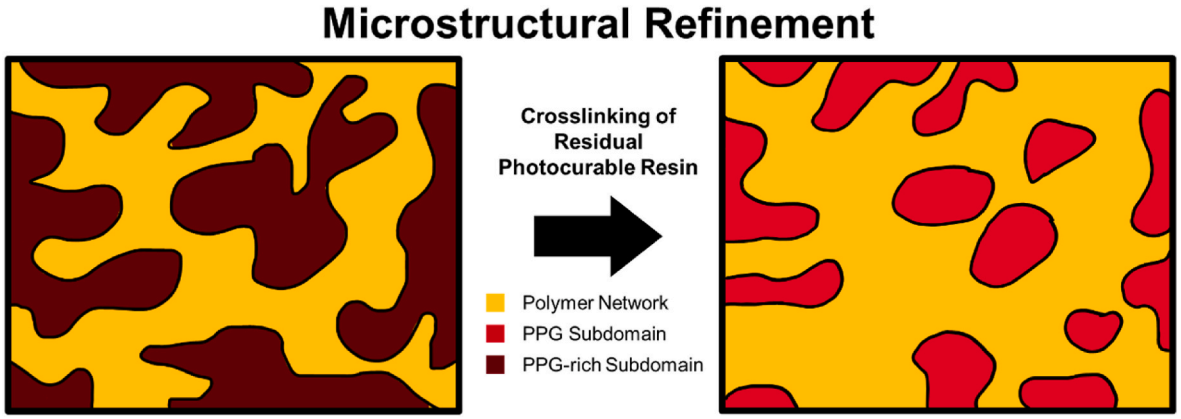

Fig. 3. Schematic illustration of mechanism 3: microstructural refinement. In the phase-separated material, PPG-rich subdomains are present containing some amount of residual uncured monomer resin. As photopolymerization progresses further, this residual resin is crosslinked with the surrounding network which results in smaller PPG subdomains.

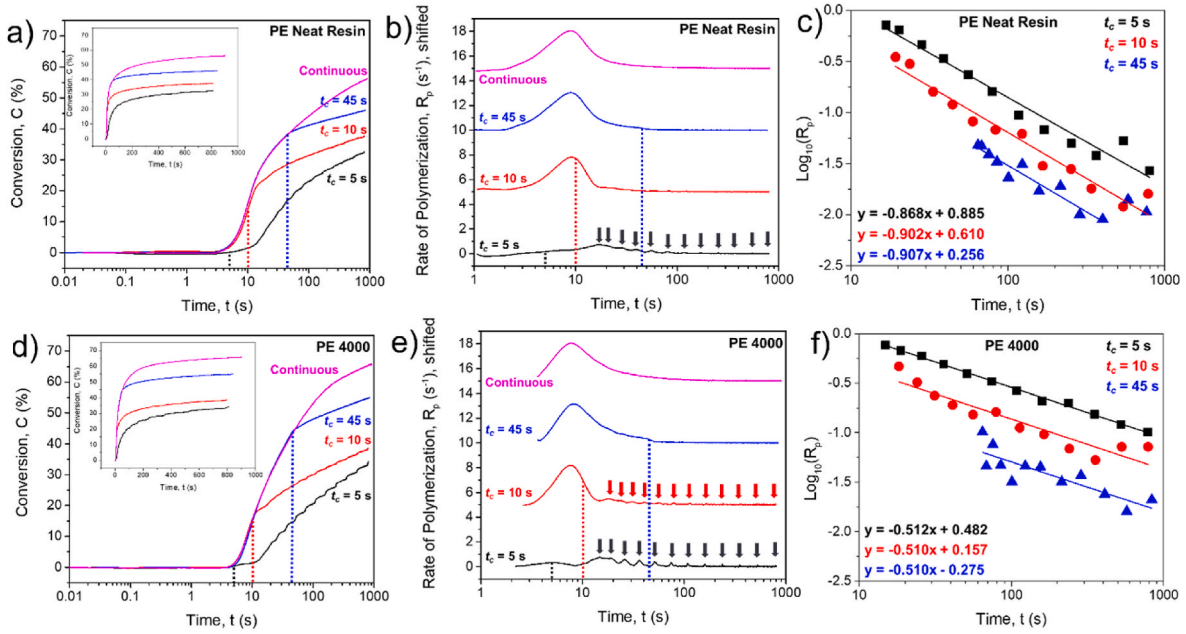

Fig. 4. Intermittent irradiation real-time FTIR monomer conversion curves for various cutoffs, t_c, for (a) the PE neat resin and (d) the PE 4000 resin. The corresponding rate of polymerization curves are shown in (b) and (e), respectively (curves shifted in the vertical direction for clarity). The rate of polymerization vs. time for $t > t_c$ and $t_c = 5$, 10 and 45 s, is shown in semi-logarithmic coordinates in (c) for the PE neat resin and in (f) for the PE 4000 resin. All systems are irradiated with 4.9 mW/cm^2 light intensity. The dotted lines designate the time at which light irradiation has ceased.

monomer conversion obtained in the systems in which irradiation is stopped is much lower than that of the continuously irradiated system, as expected. Fig. 4b shows the rate of polymerization (derivative of the conversion curves, R_p) over time. It is seen that most systems have negligible rates at the times when probing is performed; an exception to this is the $t_c = 5$ s system. In this case, multiple small peaks in the rate of polymerization can be seen in Fig. 4b and e (indicated by arrows) which indicate that TPO consumption does in fact occur due to probing in this particular system in the early stages of network development.

In Fig. 4c, the rate of polymerization is plotted vs. time for $t > t_c$ for all PE neat resin intermittent irradiation cases. The plot shows that the rate of polymerization decreases as a power law in time in the regime in which no new radicals are formed, i.e. $R_p \sim t^{-q}$, where exponent q is independent of t_c [77]. However, as indicated by Fig. 4c and f, q is larger in the neat resin case ($q \sim -0.892$) than in the PE 4000 case ($q \sim -0.511$), which indicates slower dynamics in the phase-separated system. The difference is attributed to the more tortuous diffusion path for free radicals in the phase-separated microstructure.

Fig. 4d shows that a higher conversion is obtained in the PE 4000 resin relative to the PE neat resin at all light doses considered. Additionally, the small peaks in the rate of polymerization in the $t_c = 5$ and 10 s cases are more pronounced in the phase-separated material (compare Fig. 4b with 4e, and 4c with 4f). A greater variation of the rate of polymerization at all probing points is seen, compared to the PE neat resin. This observation indicates that the PE 4000 phase-separating resin has a higher degree of TPO consumption at the probing points in all intermittent irradiation cases. Therefore, it is concluded that the presence of phase separation induces an increased driving force for photopolymerization to occur in the early stages of network development, thus causing a higher amount of TPO consumption at the probing points (Fig. 4f) and a higher overall monomer conversion (Fig. 4d). A similar enhancement of the conversion in the presence of phase separation was observed in Zakrzewski et al. [75]

To better define the extent to which the short duration of exposure during probing affects structural evolution and the transmittance curve, we perform additional experiments with $t_c = 5$, 10 and 45 s, but with only one probing point at $t = 900$ s. Fig. 5 shows a comparison of the T(t) curves obtained with intermittent probing and the T(t) curves obtained with only one probing point for $t > t_c$, at the end of the investigated period, for the three values of t_c. The effect of intermittent probing on T (t) is weak in the $t_c = 5$ and 45 s cases. In these regimes, the additional light added to the system via probing may induce further TPO consumption (mechanism 2), but in the case of $t_c = 5$ s, the effect of phase separation (i.e. mechanism 1), is dominant, while in the case of $t_c = 45$ s,

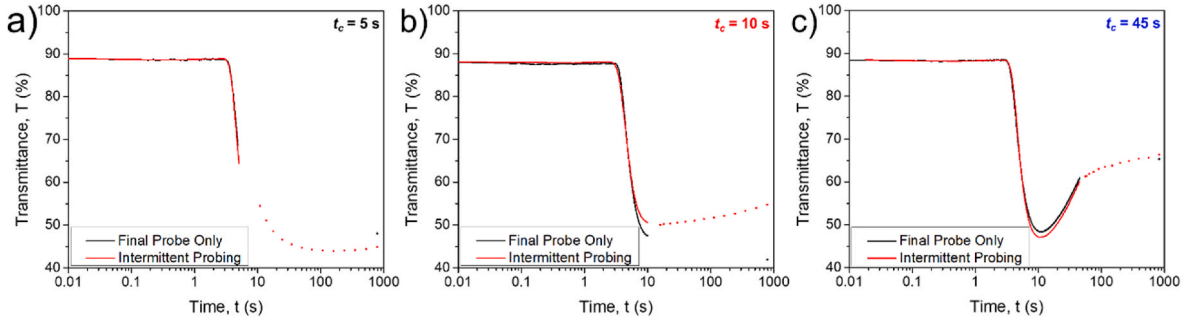

Fig. 5. Transmittance curves obtained by probing intermittently for $t > t_c$, as well as at $t = 900$ s only, for: (a) $t_c = 5$ s, (b) $t_c = 10$ s, and (c) $t_c = 45$ s. All systems are irradiated with 4.9 mW/cm^2 light intensity.

the effect of microstructural refinement (i.e. mechanism 3), is dominant. The discrepancy is more pronounced in the $t_c = 10$ s case. The intermittently probed system has a slight recovery in transmittance, while the system probed only once, at 900 s, shows a reduction in transmittance. The $t_c = 10$ s case is special in that cessation of irradiation corresponds to the minimum of the T(t) curve obtained by continuous irradiation. At that point, $dT/dt = 0$, which means that the mechanisms defining the shape of the transmittance curve balance each other exactly. In these conditions, the system becomes more sensitive to the number of radicals available in the network. Hence, the small amount of TPO consumption associated with intermittent probing is sufficient to introduce a bias favoring one mechanism or the other such to change the shape of the transmittance curve for $t > t_c$.

The effect of varying the PPG molecular weight on the phase separation process was studied in the same system and using continuous UV exposure in our previous work [75]. Phase separation is not observed when PPG with $M_n = 425$ g/mol is used, but it is observed with $M_n = 1000$ g/mol of same concentration. The drop in T(t) becomes more pronounced as M_n increases, which indicates more pronounced phase separation, but the overall shape of the respective function remains identical to that shown in Fig. 2.

3.2. Morphology of phase-separated films

The size of the phase-separated subdomains is evaluated by scanning electron microscopy (SEM) of films with surfaces treated with methanol to remove the PPG content, as described in Section 2.3. Fig. 6a shows the resulting porous morphologies of continuously irradiated samples at 5, 10, 45, 60, and 900 s of continuous light exposure. Minimal phase separation is observed at 5 s of continuous exposure and hence the etched samples have little porosity. At 10 s, the system develops a rough morphology with structures similar to those reported in other works [39,60,61]. At 45 s and later, the system retains the structure it has at 10 s, but the size of the phase-separated regions is reduced. To quantify the difference between these microstructures, we compute the coefficient of variation (CV) of the image intensity, which represents the roughness of the respective topology. This non-dimensional measure is shown for each microstructure in Fig. 6. The $t = 5$ s system has the lowest CV of 0.350, the $t = 10$ s system has the highest at 0.648, and the $t =$ 45, 60, and 900 s systems all have a similar CV around 0.579 on average, supporting the claim made above that subdomain sizes grow up to 10 s of exposure and then shrink thereafter. This data demonstrates that the PPG subdomain size is reduced due to the continuous crosslinking. Such refinement is expected to lead to a reduction of scattering and hence contributes to the increase of the transmittance at exposure times beyond the minimum of the T(t) curve, therefore substantiating mechanism 3 (Fig. 3).

Fig. 6b shows similar images for materials subjected to intermittent irradiation up to 900 s. It is seen that for all cases considered, $t_c = 5$, 10, and 45 s, the morphology closely resembles that obtained after continuous irradiation for 45, 60, and 900 s as seen in Fig. 6a. The CV values obtained for these systems also support this claim: 0.518, 0.586, and 0.526 for $t_c = 5$, 10, and 45 s, respectively. This result also suggests that in the intermittent irradiation systems, evidence of microstructural refinement is seen where the subdomain sizes are somewhat reduced and more uniform.

Volumetric contraction (shrinkage) is generally observed during curing [67–69,74,78–81]. It is of interest to determine the correlation between this process and the phenomena reported in Figs. 2 and 6. Shrinkage is calculated for each resin system after 900 s of continuous exposure and after intermittent probing for the three cutoff systems considered (t_c = 5, 10, and 45 s) using the volumetric shrinkage equation:

$$VS = [DB]_0 \times C \times SF \tag{3}$$

where VS is volumetric shrinkage, $[DB]_0$ is the double bond (-C═C) concentration, C is the monomer conversion, and SF is the shrinkage factor [82–85]. The resulting volumetric shrinkage as depicted in Table 1 portrays increasing shrinkage with increased light dose supplied to both resin systems, as expected. The more interesting factor is that the PE 4000 resin possesses a lower amount of shrinkage in the two low dose systems (t_c = 5 and 10 s). This is attributed to the interpenetrating PPG-rich subdomains causing a lower crosslink density to be obtained within the network and thus, less shrinkage to occur.

Shrinkage is also monitored in the present setup by measuring the film thickness using a profilometer. The measurement is performed after continuous exposure of $t_c = 10$, 45, 60, and 900 s at 4.9 mW/cm^2 light

Table 1
Volumetric shrinkage (%) of the PE neat and PE 4000 resins after intermittent probing (t_c = 5, 10, and 45 s) or continuous exposure for 900 s.

Irradiation Dose (mJ/cm^2)	49.98 (t_c = 5s)	74.48 (t_c = 10 s)	244.02 (t_c = 45 s)	4410 (t = 900 s)
PE Neat Resin	13.2	15.4	18.7	22.8
PE 4000	12.2	13.8	19.6	23.5

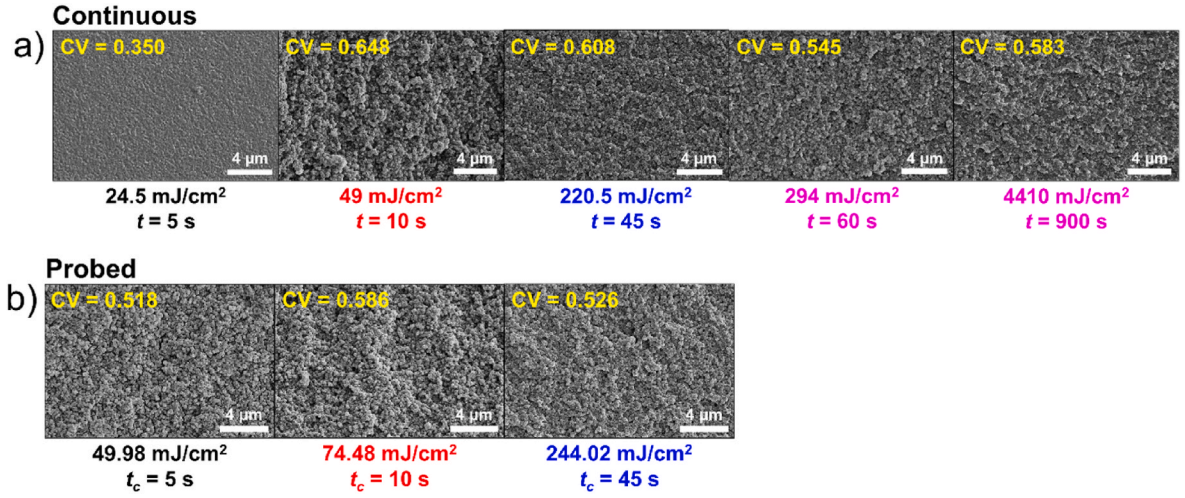

Fig. 6. SEM of the (a) continuously irradiated and (b) intermittently probed PE 4000 resin samples. All samples are irradiated using 4.9 mW/cm^2 light intensity. The total irradiation dose is reported for each image; in (b) the dose includes the contribution of intermittent probing up to 900 s of observation time. The coefficient of variation (CV) of the image intensity is also given for each image as a non-dimensional measure of roughness.

intensity (5 s is not shown as the film was underdeveloped and did not provide accurate results). Fig. 7 shows that the film thickness is maintained until 45 s and then decreases continuously for both the PE neat and PE 4000 resins. Interestingly, the thickness of films in which phase separation takes place (i.e. PE 4000), is always larger than the thickness of the PE neat resin films. This is likely because phase separation restricts contraction to some extent. This also could be directly correlated with the higher monomer conversion that is seen in the PE 4000 resin in Fig. 4. The results in Fig. 7 agree qualitatively with those in Table 1.

According to Fig. 7, a sharp decrease of the film thickness takes place at approximately 45 s of exposure, or a dose of 220 mJ/cm^2. This irradiation time corresponds to the microstructural refinement observed in Fig. 6—a stage of the T(t) curve in which mechanism 3 dominates. Beyond this time, the crosslink density increases leading to continuous network collapse. This increases the network homogeneity, decreases scattering, and increases the transmittance. We infer that the rapid increase in transmittance seen from 10 to 45 s in the continuous curve of PE 4000 (Fig. 2a), is due to the increasing homogeneity of the network in the un-collapsed state via mechanism 3. After this point, collapse begins to occur, being fully achieved by ~300 s, causing the transmittance to flatten out. This also agrees with the extent of monomer conversion seen in Fig. 4d where conversion also flattens out at ~300 s. However, this disagrees with the system studied by Kimura et al. [67] In their work, it was found that in phase-separating PSAF/MMA mixtures, phase separation occurred at the same time at which network shrinkage achieved equilibrium [67]. In our case, this would be at ~300 s. But it is known through Fig. 2 that phase separation is complete in our system at this stage. The work of Tran-Cong-Miyata et al. [68] on the other hand, supports our claim since their systems of PEA-AR/MMA phase separated prior to network shrinkage.

Our data indicates that the increase in transmittance of the PE 4000 resin is due to a combination of microstructural refinement associated with continuous crosslinking (mechanism 3) and, to a smaller extent, to TPO consumption (mechanism 2).

3.3. Light intensity dependence of phase separation kinetics

As previously demonstrated, varying the light intensity alters the phase separation kinetics [75]. Increasing the light intensity enables faster photopolymerization, but consequently, a smaller amount of phase separation results due to partial entrapment of the polymer additive chains. This effect of light intensity is illustrated in Fig. 8 by comparing the reference data from Figs. 2 and 4 obtained with light intensity of 4.9 mW/cm^2 with similar data obtained by using an intensity of 1.3 mW/cm^2.

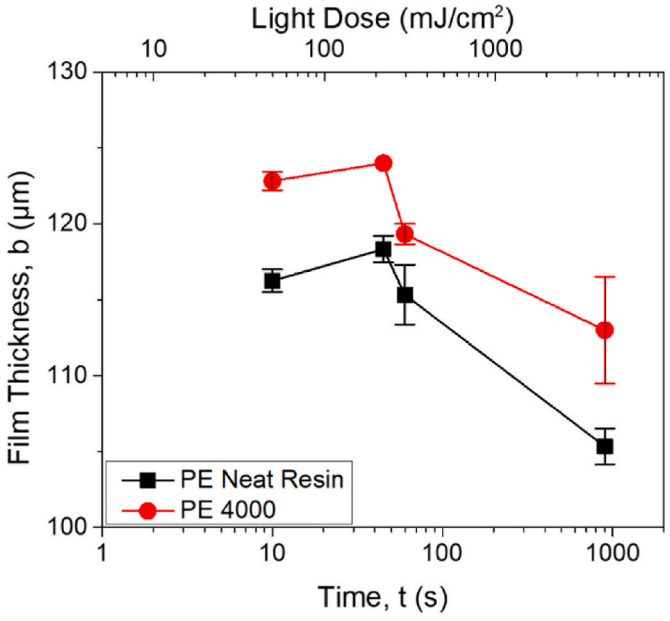

Fig. 7. Film thickness versus light dose of the PE neat and PE 4000 resins measured via profilometry after continuous irradiation with exposure times of 10, 45, 60, and 900 s and a light intensity of 4.9 mW/cm^2.

The transmittance curves at the two light intensities of 1.3 and 4.9 mW/cm^2 are shown in Fig. 8a for the phase-separating PE 4000 resin. The change in transmittance from the induction time of phase separation to the minimum of the transmittance curve (occurring at t ~ 30 s for 1.3 mW/cm^2 and t ~ 10 s for 4.9 mW/cm^2), is larger at the lower light intensity of 1.3 mW/cm^2. This indicates that phase separation occurs to a larger extent at a lower light intensity due to the reduced photopolymerization kinetics, agreeing with Yamashita et al. [60] and our previous findings [75]. The induction time of phase separation is smaller when using the larger intensity of 4.9 mW/cm^2, which indicates faster phase separation kinetics at a higher light intensity.

Fig. 8b shows the monomer conversion curves at two light intensities of 1.3 and 4.9 mW/cm^2 for the phase-separating PE 4000 resin, obtained via real-time FTIR. The lower intensity is unable to polymerize to the same extent as the higher intensity, which is expected due to the lower overall dose of light supplied to the system. Additionally, the induction time of photopolymerization (denoted by the upturn in the conversion curves), is smaller at the higher intensity of 4.9 mW/cm^2. Furthermore, the rates of polymerization shown in Fig. 8c further validate that the kinetics of photopolymerization is much faster at the higher light intensity. Moreover, the induction times of phase separation for both intensities of 1.3 and 4.9 mW/cm^2 obtained from transmittance are approximately identical to the respective induction times of photopolymerization obtained from real-time FTIR. Therefore, phase separation and photopolymerization occur simultaneously at both light intensities considered.

In order to investigate whether the phase separation process at the lower light intensity of 1.3 mW/cm^2 occurs differently than in the previously examined 4.9 mW/cm^2 intensity case, additional intermittent irradiation transmittance experiments are performed. These experiments are identical to those performed for the 4.9 mW/cm^2 case, except the continuous exposure durations are altered due to the slower kinetics at this low intensity, i.e. $t_c = 15$, 30, and 105 s. After these durations, the light is turned off and only turned back on intermittently for 0.4 s at intervals equally spaced on a 1.5x log-scale.

In the $t_c = 15$ s case and using 1.3 mW/cm^2 intensity, T(t) decreases continuously for $t > t_c$ (Fig. 9), which indicates that phase separation continues to develop even after light exposure has ceased. This situation is similar to the $t_c = 5$ s and 4.9 mW/cm^2 case (Fig. 2a), which corresponds to approximately the same dose provided to the sample during continuous irradiation. For $t_c = 30$ s, which corresponds to the minimum of the transmittance curve, for $t > t_c$, transmittance remains approximately constant, which is in qualitative agreement with the 4.9 mW/cm^2 case with $t_c = 10$ s. When $t_c = 105$ s, T(t) shows an increasing trend for $t > t_c$, indicating increased network development and microstructural refinement via mechanism 3, similar to the $t_c = 45$ s and 4.9 mW/cm^2 system. Through all of this, it is seen that phase separation occurs in mainly the same manner at various light intensities when the same dose is provided to the sample during the continuous exposure period, $t < t_c$. An essential difference though is that TPO consumption occurring during probing is more significant at a higher light intensity. Further information on this light intensity variation during probing is given in Section 4 of the SI.

4. Conclusion

In this work, the evolution of phase separation during photopolymerization-induced phase separation (photo-PIPS) in a photocurable resin was analyzed by halting network development and using intermittent irradiation probing. Transmittance tests show that during

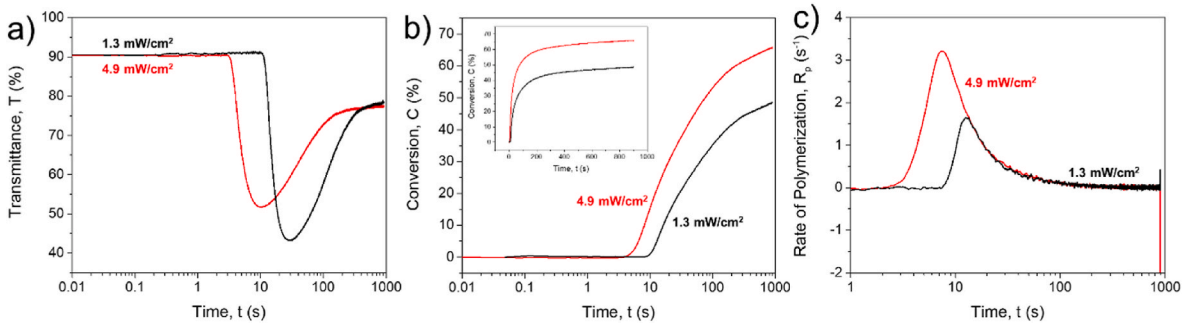

Fig. 8. (a) Light transmittance curves for the PE 4000 resin at two light intensities. (b) The monomer conversion and (c) rate of polymerization measured via real-time FTIR for the PE 4000 resin at 1.3 and 4.9 mW/cm^2.

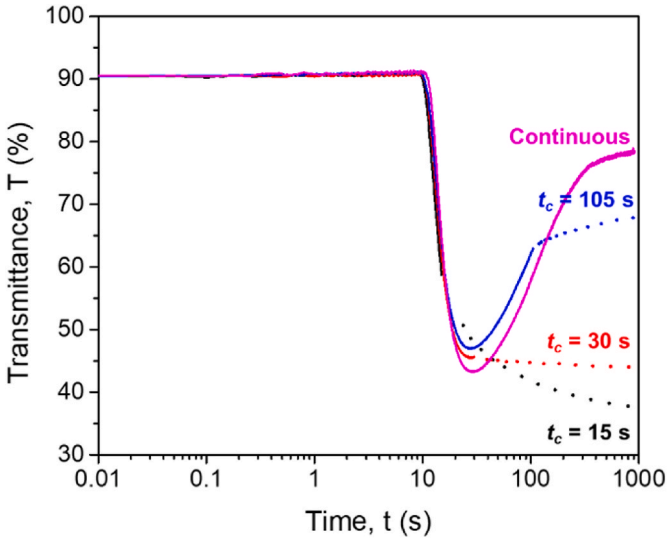

Fig. 9. Intermittent irradiation transmittance curves for the cutoff times of t_c = 15, 30, and 105 s using a light intensity of 1.3 mW/cm^2.

photopolymerization of our phase-separating resin, a rapid reduction in transmittance occurs, which indicates the onset of phase separation due to light scattering. The transmittance ultimately reaches a minimum point at which phase separation is at a maximum, and then shows recovery to higher percent transmittance. To study this behavior, the phase-separating resin was irradiated for various durations of light exposure and then probed intermittently to allow for examination of the system at different stages of the phase separation process. Real-time FTIR experiments were performed to validate the significance of TPO photoinitiator consumption (mechanism 2), at $t > t_c$, on network development. It was seen that at higher light intensities, intermittent probing induces further TPO consumption, potentially changing the way the network evolves. Light transmittance experiments in these intermittent systems indicated that at the early stages of network development, i.e. $t_c = 5$ s, phase separation (mechanism 1), is the predominant mechanism governing the microstructure. At $t_c = 10$ s, mechanisms 1 and 3 (phase separation and microstructural refinement), are in balance with one another. At $t_c = 45$ s, mechanism 3 supersedes mechanism 1 and light transmittance increases. SEM experiments validated the occurrence of microstructural refinement through the morphology changes from 10 to 45 s of irradiation. Further, the film thicknesses of continuously irradiated samples were measured via profilometry. It was found that film collapse begins to occur after 45 s of exposure and is complete by ~300 s. This was supported by the plateaued regions in both the monomer conversion and continuous transmittance curves.

It is concluded that during the photo-PIPS process, phase separation is the predominant mechanism governing the microstructure evolution at the early stages in network development. From there, microstructural refinement occurs as residual monomer resin within the phase-separated subdomains gradually crosslinks with the surrounding network. This information can be used to further understand the parameters controlling the resulting microstructure of materials developed using photo-PIPS, allowing for full control on microstructural development and material properties.

CRediT authorship contribution statement

Lauren Zakrzewski: Conceptualization, Data curation, Investigation, Methodology, Writing – original draft. **Chang Y. Ryu:** Conceptualization, Funding acquisition. **Chulsung Bae:** Supervision. **Catalin R. Picu:** Conceptualization, Formal analysis, Funding acquisition, Investigation, Project administration, Writing – review & editing.

Declaration of competing interest

The authors declare that they have no known competing financial interests or personal relationships that could have appeared to influence the work reported in this paper.

Data availability

Data will be made available on request.

Acknowledgment

This research was supported by the NSF through grant CMMI-2007909.

Appendix A. Supplementary data

Supplementary data to this article can be found online at https://doi.org/10.1016/j.polymer.2023.126526.

References

[1] W. Wei, G. Chen, S. Li, X. Zhou, H. Peng, X. Xie, Y.-W. Mai, Computational insight into phase separation of a thiol-ene photopolymer with liquid crystals for holography by dissipative particle dynamics simulation, Macromolecules 56 (14) (2023) 5457–5469, https://doi.org/10.1021/acs.macromol.3c00251.
[2] Y. Zhao, X. Zhao, M. Li, Z. Li, H. Peng, X. Xie, Crosstalk-free patterning of cooperative-thermoresponse images by the synergy of the AIEgen with the liquid crystal, Angew. Chem. Int. Ed. 59 (25) (2020) 10066–10072, https://doi.org/10.1002/anie.201915053.
[3] Y. Zhao, H. Peng, X. Zhou, Z. Li, X. Xie, Interfacial AIE for orthogonal integration of holographic and fluorescent dual-thermosensitive images, Adv. Sci. 9 (10) (2022), 2105903, https://doi.org/10.1002/advs.202105903.
[4] Y.-X. Hu, X. Hao, L. Xu, X. Xie, B. Xiong, Z. Hu, H. Sun, G.-Q. Yin, X. Li, H. Peng, H.-B. Yang, Construction of supramolecular liquid-crystalline metallacycles for holographic storage of colored images, J. Am. Chem. Soc. 142 (13) (2020) 6285–6294, https://doi.org/10.1021/jacs.0c00698.

[5] M. Yao, Y. Zhao, X. Zhou, Z. Li, H. Peng, X. Xie, Orthogonal integration of holographic and fluorescent dual images based on energy transfer from liquid crystals to a photocleavable AIEgen, J Mater Chem C Mater 11 (10) (2023) 3504–3512, https://doi.org/10.1039/D2TC05387J.

[6] J. Lu, R.P. Wool, Additive toughening effects on new bio-based thermosetting resins from plant oils, Compos. Sci. Technol. 68 (2008) 1025–1033, https://doi.org/10.1016/j.compscitech.2007.07.009.

[7] B.S. Hayes, J.C. Seferis, Modification of thermosetting resins and composites through preformed polymer particles: a review, Polym. Compos. 22 (4) (2001) 451–467, https://doi.org/10.1002/pc.10551.

[8] A.V. Pocius, Elastomer modification of structural adhesives, Rubber Chem. Technol. 58 (3) (1985) 622–636, https://doi.org/10.5254/1.3536081.

[9] K. Liu, C.W. Macosko, Can nanoparticle toughen fiber-reinforced thermosetting polymers? J. Mater. Sci. 54 (2019) 4471–4483, https://doi.org/10.1007/s10853-018-03195-9.

[10] Y. Huang, D.L. Hunston, A.J. Kinloch, C.K. Riew, Mechanisms of toughening thermoset resins, Advances in Chemistry 233 (1993) 1–35, https://doi.org/10.1021/ba-1993-0233.ch001.

[11] R.J.J. Williams, B.A. Rozenberg, J.-P. Pascault, Reaction-induced phase separation in modified thermosetting polymers, Adv. Polym. Sci. 128 (1997) 95–156.

[12] X. Bian, R. Tuo, W. Yang, Y. Zhang, Q. Xie, J. Zha, J. Lin, S. He, Mechanical, thermal, and electrical properties of BN-epoxy composites modified with carboxyl-terminated butadiene nitrile liquid rubber, Polymers 11 (10) (2019) 1548, https://doi.org/10.3390/polym11101548.

[13] S.C. Ligon-Auer, M. Schwentenwein, C. Gorsche, J. Stampfl, R. Liska, Toughening of photo-curable polymer networks: a review, Polym. Chem. 7 (2) (2016) 257–286, https://doi.org/10.1039/c5py01631b.

[14] J. Parameswaranpillai, N. Hameed, J. Pionteck, E.M. Woo, Handbook of Epoxy Blends, Springer International Publishing, 2016, https://doi.org/10.1007/978-3-319-18158-5.

[15] T.H. Hsieh, A.J. Kinloch, A.C. Taylor, S. Sprenger, The effect of silica nanoparticles and carbon Nanotubes on the toughness of a thermosetting epoxy polymer, J. Appl. Polym. Sci. 119 (4) (2011) 2135–2142, https://doi.org/10.1002/app.32937.

[16] V. Sorichetti, V. Hugouvieux, W. Kob, Dynamics of nanoparticles in polydisperse polymer networks: from free diffusion to hopping, Macromolecules 54 (18) (2021) 8575–8589, https://doi.org/10.1021/acs.macromol.1c01394.

[17] O. Zabihi, A. Hooshafza, F. Moztarzadeh, H. Payravand, A. Afshar, R. Alizadeh, Isothermal curing behavior and thermo-physical properties of epoxy-based thermoset nanocomposites reinforced with Fe2O3 nanoparticles, Thermochim. Acta 527 (2012) 190–198, https://doi.org/10.1016/j.tca.2011.10.026.

[18] O. Zabihi, A. Khodabandeh, S.M. Mostafavi, Preparation, optimization and thermal characterization of a novel conductive thermoset nanocomposite containing polythiophene nanoparticles using dynamic thermal analysis, Polym. Degrad. Stabil. 97 (1) (2012) 3–13, https://doi.org/10.1016/j.polymdegradstab.2011.10.022.

[19] Y. Tang, L. Ye, Z. Zhang, K. Friedrich, Interlaminar fracture toughness and CAI strength of fibre-reinforced composites with nanoparticles - a review, Compos. Sci. Technol. 86 (2013) 26–37, https://doi.org/10.1016/j.compscitech.2013.06.021.

[20] B.H. Fan, J.W. Zha, D.R. Wang, J. Zhao, Z.F. Zhang, Z.M. Dang, Preparation and dielectric behaviors of thermoplastic and thermosetting polymer nanocomposite films containing BaTiO3 nanoparticles with different diameters, Compos. Sci. Technol. 80 (2013) 66–72, https://doi.org/10.1016/j.compscitech.2013.02.021.

[21] J.D. Clapper, J.M. Skeie, R.F. Mullins, C.A. Guymon, Development and characterization of photopolymerizable biodegradable materials from PEG-PLA-PEG block macromonomers, Polymer (Guildf) 48 (22) (2007) 6554–6564, https://doi.org/10.1016/j.polymer.2007.08.023.

[22] P.M. Lipic, F.S. Bates, M.A. Hillmyer, Nanostructured thermosets from self-assembled amphiphilic block copolymer/epoxy resin mixtures, J. Am. Chem. Soc. 120 (1998) 8963–8970.

[23] Y. Mai, A. Eisenberg, Self-assembly of block copolymers, Chem. Soc. Rev. 41 (18) (2012) 5969–5985, https://doi.org/10.1039/c2cs35115c.

[24] T.P. Lodge, Block copolymers: past successes and future challenges, Macromol. Chem. Phys. 204 (2) (2003) 265–273, https://doi.org/10.1002/macp.200290073.

[25] A. Bonnet, J.P. Pascault, H. Sautereau, M. Taha, Y. Camberlin, Epoxy-diamine thermoset/thermoplastic blends. 1. Rates of reactions before and after phase separation, Macromolecules 32 (25) (1999) 8517–8523, https://doi.org/10.1021/ma981754p.

[26] R.C. Willemse, E.J.J. Ramaker, J. Van Dam, A. Posthuma De Boer, Morphology development in immiscible polymer blends: initial blend morphology and phase dimensions, Polymer (Guildf) 40 (1999) 6651–6659.

[27] H. Veenstra, J. Van Dam, A. Posthuma De Boer, On the coarsening of Co-continuous morphologies in polymer blends: effect of interfacial tension, viscosity and physical cross-links, Polymer (Guildf) 41 (2000) 3037–3045.

[28] K. Murata, J. Sachin, H. Etori, T. Anazawa, Photopolymerization-induced phase separation in binary blends of photocurable/linear polymers, Polymer (Guildf) 43 (2002) 2845–2859.

[29] Y. Sasaki, N. Aiba, H. Hashimoto, J. Kumaki, Reversible hierarchical phase separation of a poly(methyl methacrylate) and poly(n -Nonyl acrylate) blend in a Langmuir monolayer, Macromolecules 43 (21) (2010) 9077–9086, https://doi.org/10.1021/ma102027t.

[30] N. Naderi, S. Rastegar, M. Mohseni, M. Khorasani, Controlling final morphologies of two-step polymerization induced phase separated blends of trimethylolpropane triacrylate/acrylate copolymer through copolymer molecular weight, Polym. Test. 61 (2017) 146–149, https://doi.org/10.1016/j.polymertesting.2017.04.002.

[31] N. Naderi, S. Rastegar, M. Mohseni, M. Khorasani, Photo-polymerization induced viscoelastic phase separation of trimethylolpropane triacrylate/poly (Styrene-Co-Methyl methacrylate) blends, Polymer (Guildf) 153 (2018) 391–397, https://doi.org/10.1016/j.polymer.2018.03.038.

[32] C.R. Szczepanski, J.W. Stansbury, Modification of linear prepolymers to tailor heterogeneous network formation through photo-initiated polymerization-induced phase separation, Polymer (Guildf) 70 (2015) 8–18, https://doi.org/10.1016/j.polymer.2015.06.002.

[33] H.M.J. Boots, J.G. Kloosterboer, C. Serbutoviez, F.J. Touwslager, Polymerization-induced phase separation. 1. Conversion-phase diagrams, Macromolecules 29 (1996) 7683–7689.

[34] W. Li, L.J. Lee, Low temperature cure of unsaturated polyester resins with thermoplastic additives I. Dilatometry and morphology study, Polymer (Guildf) 41 (2000) 685–696.

[35] I.J. Roh, S. Ramaswamy, W.B. Krantz, A.R. Greenberg, Poly(Ethylene Chlorotrifluoroethylene) membrane formation via thermally induced phase separation (TIPS), J. Membr. Sci. 362 (1–2) (2010) 211–220, https://doi.org/10.1016/j.memsci.2010.06.042.

[36] J. Wang, L. Wang, W. Ruan, C. Zhang, J. Ji, Rheology behavior of high-density polyethylene/diluent blends and fabrication of hollow-fiber membranes via thermally induced phase separation, J. Appl. Polym. Sci. 118 (4) (2010) 2186–2194, https://doi.org/10.1002/app.32584.

[37] Y. Zhang, F. Chen, W. Shi, Y. Liang, C.C. Han, Layered structure formation in the reaction-induced phase separation of epoxy/polysulfone blends, Polymer (Guildf) 51 (25) (2010) 6030–6036, https://doi.org/10.1016/j.polymer.2010.10.027.

[38] C. Zhang, Y. Bai, Y. Sun, J. Gu, Y. Xu, Preparation of hydrophilic HDPE porous membranes via thermally induced phase separation by blending of amphiphilic PE-b-PEG copolymer, J. Membr. Sci. 365 (1–2) (2010) 216–224, https://doi.org/10.1016/j.memsci.2010.09.007.

[39] M. Seo, M.A. Hillmyer, Reticulated nanoporous polymers by controlled polymerization-induced microphase separation, Science 336 (6087) (1979) 1422–1425, https://doi.org/10.1126/science.1221383, 2012.

[40] A. Hara, R. Inoue, N. Takahashi, K. Nishida, T. Kanaya, Trajectory of critical point in polymerization-induced phase separation of epoxy/oligoethylene glycol solutions, Macromolecules 47 (13) (2014) 4453–4459, https://doi.org/10.1021/ma5009258.

[41] M.W. Schulze, L.D. McIntosh, M.A. Hillmyer, T.P. Lodge, High-modulus, high-conductivity nanostructured polymer electrolyte membranes via polymerization-induced phase separation, Nano Lett. 14 (1) (2014) 122–126, https://doi.org/10.1021/nl4034818.

[42] A.H. Torbati, H.B. Nejad, M. Ponce, J.P. Sutton, P.T. Mather, Properties of triple shape memory composites prepared via polymerization-induced phase separation, Soft Matter 10 (17) (2014) 3112–3121, https://doi.org/10.1039/c3sm52599f.

[43] X. Yi, L. Kong, X. Dong, X. Zuo, X. Kuang, Z. Feng, D. Wang, Polymerization induced viscoelastic phase separation of porous phenolic resin from solution, Polym. Int. 65 (9) (2016) 1031–1038, https://doi.org/10.1002/pi.5147.

[44] Y. Ding, Q. Zhao, L. Wang, L. Huang, Q. Liu, X. Lu, Y. Cai, Polymerization-induced self-assembly promoted by liquid-liquid phase separation, ACS Macro Lett. 8 (8) (2019) 943–946, https://doi.org/10.1021/acsmacrolett.9b00435.

[45] P. Zhang, Z. Gao, Q. Zhang, A. Khattab, G. Li, Fracture behavior characterization of arcan polycaprolactone based polymer composites prepared by polymerization induced phases separation, Polym. Compos. 40 (3) (2019) 1198–1208, https://doi.org/10.1002/pc.24831.

[46] P. Zhang, D.C. Sundberg, J.G. Tsavalas, Polymerization induced phase separation in composite latex particles during seeded emulsion polymerization, Ind. Eng. Chem. Res. 58 (2019) 21118–21129, https://doi.org/10.1021/acs.iecr.9b02964.

[47] C. Kahrs, T. Gühlstorf, J. Schwellenbach, Influences of different preparation variables on polymeric membrane formation via nonsolvent induced phase separation, J. Appl. Polym. Sci. 137 (28) (2020), https://doi.org/10.1002/app.48852.

[48] M. Pavlovic, M. Antonietti, B.V.K.J. Schmidt, L. Zeininger, Responsive Janus and Cerberus emulsions via temperature-induced phase separation in aqueous polymer mixtures, J. Colloid Interface Sci. 575 (2020) 88–95, https://doi.org/10.1016/j.jcis.2020.04.067.

[49] Y. Tang, K. Wu, S. Yu, J. Chen, X. Ding, L. Rao, Z. Li, Bioinspired high-scattering polymer films fabricated by polymerization-induced phase separation, Opt. Lett. 45 (10) (2020), https://doi.org/10.1364/ol.390639, 2918–1921.

[50] F. Wang, L. Ratke, H. Zhang, P. Altschuh, B. Nestler, A phase-field study on polymerization-induced phase separation occasioned by diffusion and capillary flow—a mechanism for the formation of porous microstructures in membranes, J. Sol. Gel Sci. Technol. 94 (2) (2020) 356–374, https://doi.org/10.1007/s10971-020-05238-7.

[51] S. Aoshima, H. Oda, E. Kobayashi, Synthesis of thermally-induced phase separating polymer with well-defined polymer structure by living cationic polymerization. I. Synthesis of poly(Vinyl Ether)s with oxyethylene units in the pendant and its phase separation behavior in aqueous solution, J. Polym. Sci. Polym. Chem. 30 (11) (1992) 2407–2413, https://doi.org/10.1002/pola.1992.080301115.

[52] F. Dan, C. Vasiliu-Oprea, Anionic polymerization of caprolactam in organic media. Morphological aspects, Colloid Polym. Sci. 276 (6) (1998) 483–495, https://doi.org/10.1007/s003960050270.

[53] C. Serbutoviez, J.G. Kloosterboer, H.M.J. Boots, F.J. Touwslager, Polymerization-induced phase separation. 2. Morphology of polymer-dispersed liquid crystal thin films, Macromolecules 29 (1996) 7690–7698.

[54] J. Yao, M. Takahashi, T. Yoko, Controlled preparation of macroporous TiO2 films by photo polymerization-induced phase separation method and their photocatalytic performance, Thin Solid Films 517 (24) (2009) 6479–6485, https://doi.org/10.1016/j.tsf.2009.03.214.

[55] W. Wang, Y. Pan, K. Shi, C. Peng, X. Ji, Hierarchical porous polymer beads prepared by polymerization-induced phase separation and emulsion-template in a microfluidic device, Chin. J. Polym. Sci. 32 (12) (2014) 1646–1654, https://doi.org/10.1007/s10118-014-1547-1.
[56] R.J.J. Williams, C.E. Hoppe, I.A. Zucchi, H.E. Romeo, I.E. dell'Erba, M.L. Gómez, J. Puig, A.B. Leonardi, Self-assembly of nanoparticles employing polymerization-induced phase separation, J. Colloid Interface Sci. 431 (2014) 223–232, https://doi.org/10.1016/j.jcis.2014.06.022.
[57] C.R. Szczepanski, J.W. Stansbury, Accessing photo-based morphological control in phase-separated, cross-linked networks through delayed gelation, Eur. Polym. J. 67 (2015) 314–325, https://doi.org/10.1016/j.eurpolymj.2015.04.006.
[58] E. Kemiklioglu, L.C. Chien, Effects of photoinitiator on electro-optical properties of polymerization-induced phase separation blue-phase liquid crystals, European Physical Journal E 40 (4) (2017), https://doi.org/10.1140/epje/i2017-11524-6.
[59] S. Guo, G. Kang, D.T. Phan, M.N. Hsu, Y.C. Por, C.H. Chen, Polymerization-induced phase separation formation of structured hydrogel particles via microfluidics for scar therapeutics, Sci. Rep. 8 (1) (2018) 2245, https://doi.org/10.1038/s41598-018-20516-9.
[60] Y. Yamashita, K. Komori, T. Murata, H. Nakanishi, T. Norisuye, T. Yamao, Q. Tran-Cong-Miyata, Conducting polymer networks synthesized by photopolymerization-induced phase separation, Adv. Nat. Sci. Nanosci. Nanotechnol. 9 (1) (2018), 015009, https://doi.org/10.1088/2043-6254/aaabae.
[61] D.G. Moore, L. Barbera, K. Masania, A.R. Studart, Three-dimensional printing of multicomponent glasses using phase-separating resins, Nat. Mater. 19 (2) (2020) 212–217, https://doi.org/10.1038/s41563-019-0525-y.
[62] H. Kihara, T. Miura, Morphology of a hydrogen-bonded LC polymer prepared by photopolymerization- induced phase separation under an isotropic phase, Polymer (Guildf) 46 (23) (2005) 10378–10382, https://doi.org/10.1016/j.polymer.2005.08.068.
[63] S. Park, H.K. Kim, J.W. Hong, Investigation of the photopolymerization-induced phase separation process in polymer dispersed liquid crystal, Polym. Test. 29 (7) (2010) 886–893, https://doi.org/10.1016/j.polymertesting.2010.05.015.
[64] D.M. Smith, C.Y. Li, T.J. Bunning, Light-directed mesoscale phase separation via holographic polymerization, J. Polym. Sci. B Polym. Phys. 52 (3) (2014) 232–250, https://doi.org/10.1002/polb.23413.
[65] F. Wang, J. Tang, C. Liu, W. Xiang, K. Wang, K. Wang, Facile fabrication of porous cross-linked monolith based on nature soybean oil by low temperature phase separation photopolymerization, J. Porous Mater. 24 (4) (2017) 991–996, https://doi.org/10.1007/s10934-016-0338-1.
[66] T. Shukutani, T. Myojo, H. Nakanishi, T. Norisuye, Q. Tran-Cong-Miyata, Tricontinuous morphology of ternary polymer blends driven by photopolymerization: reaction and phase separation kinetics, Macromolecules 47 (13) (2014) 4380–4386, https://doi.org/10.1021/ma500302k.
[67] N. Kimura, K. Kawazoe, H. Nakanishi, T. Norisuye, Q. Tran-Cong-Miyata, Influences of wetting and shrinkage on the phase separation process of polymer mixtures induced by photopolymerization, Soft Matter 9 (35) (2013) 8428–8437, https://doi.org/10.1039/c3sm51203g.
[68] Q. Tran-Cong-Miyata, T. Kinohira, D.T. Van-Pham, A. Hirose, T. Norisuye, H. Nakanishi, Phase separation of polymer mixtures driven by photochemical reactions: complexity and fascination, Curr. Opin. Solid State Mater. Sci. 15 (6) (2011) 254–261, https://doi.org/10.1016/j.cossms.2011.06.004.
[69] A. Hirose, K. Shimada, C. Hayashi, H. Nakanishi, T. Norisuye, Q. Tran-Cong-Miyata, Polymer networks with bicontinuous gradient morphologies resulting from the competition between phase separation and photopolymerization, Soft Matter 12 (6) (2016) 1820–1829, https://doi.org/10.1039/c5sm02399h.
[70] P.K. Chan, A.D. Rey, Polymerization-induced phase separation. 1. Droplet size selection mechanism, Macromolecules 29 (1996) 8934–8941.
[71] P.K. Chan, A.D. Rey, Polymerization-induced phase separation. 2. Morphological analysis, Macromolecules 30 (1997) 2135–2143.
[72] T.-S. Chung, The limitations of using flory-huggins equation for the states of solutions during asymmetric hollow-fiber formation, J. Membr. Sci. 126 (1997) 19–34.
[73] M. Abouhamzeh, J. Sinke, R. Benedictus, Prediction models for distortions and residual stresses in thermoset polymer laminates: an overview, Journal of Manufacturing and Materials Processing 3 (4) (2019) 87, https://doi.org/10.3390/jmmp3040087.
[74] P. Prasatya, G.B. McKenna, S.L. Simon, A viscoelastic model for predicting isotropic residual stresses in thermosetting materials: effects of processing parameters, J. Compos. Mater. 35 (10) (2001) 826–848, https://doi.org/10.1106/D0JJ-V6Q1-891M-3GJR.
[75] L. Zakrzewski, Y. Kim, Y. Song, C.Y. Ryu, C. Bae, C.R. Picu, Interplay of photopolymerization and phase separation kinetics and the resulting structure-property relationship of photocurable resins, Polymer (Guildf) 280 (2023), 126032, https://doi.org/10.1016/j.polymer.2023.126032.
[76] Y. Kim, Y. Song, C.Y. Ryu, C. Bae, C.R. Picu, Reactive UV Transmittance Analysis in Photopolymerization Induced Phase Separation, 2023. *Manuscript in Preparation*.
[77] A. Goto, T. Fukuda, Kinetics of living radical polymerization, Prog. Polym. Sci. 29 (4) (2004) 329–385, https://doi.org/10.1016/j.progpolymsci.2004.01.002.
[78] D. Karalekas, D. Rapti, E.E. Gdoutos, A. Aggelopoulos, Investigation of shrinkage-induced stresses in stereolithography photo-curable resins, Exp. Mech. 42 (4) (2002) 439–444.
[79] J.P. Fouassier, J. Lalevée, Photoinitiators for Polymer Synthesis: Scope, Reactivity and Efficiency, Wiley, 2012, https://doi.org/10.1002/9783527648245.
[80] H.J. Lee, H.Y. Park, E.H. Kim, H.H. Choi, J. Jin, J. Choi, S.C. Yang, Y.G. Jung, Relationship between mechanical properties of ceramic green body and structures of photo-cured acrylate polymer for ceramic 3D printing based on photo polymerization, Ceram. Int. 47 (3) (2021) 3867–3875, https://doi.org/10.1016/j.ceramint.2020.09.247.
[81] M. Dewaele, D. Truffier-Boutry, J. Devaux, G. Leloup, Volume contraction in photocured dental resins: the shrinkage-conversion relationship revisited, Dent. Mater. 22 (4) (2006) 359–365, https://doi.org/10.1016/j.dental.2005.03.014.
[82] S. Ye, N.B. Cramer, I.R. Smith, K.R. Voigt, C.N. Bowman, Reaction kinetics and reduced shrinkage stress of thiol-yne-methacrylate and thiol-yne-acrylate ternary systems, Macromolecules 44 (23) (2011) 9084–9090, https://doi.org/10.1021/ma2018809.
[83] H. Peng, D.P. Nair, B.A. Kowalski, W. Xi, T. Gong, C. Wang, M. Cole, N.B. Cramer, X. Xie, R.R. McLeod, C.N. Bowman, High performance graded rainbow holograms via two-stage sequential orthogonal thiol-click chemistry, Macromolecules 47 (7) (2014) 2306–2315, https://doi.org/10.1021/ma500167x.
[84] H. Lu, J.A. Carioscia, J.W. Stansbury, C.N. Bowman, Investigations of step-growth thiol-ene polymerizations for novel dental restoratives, Dent. Mater. 21 (12) (2005) 1129–1136, https://doi.org/10.1016/j.dental.2005.04.001.
[85] M.P. Patel, M. Braden, K.W.M. Davy, Polymerization shrinkage of methacrylate esters, Biomaterials 8 (1) (1987) 53–56, https://doi.org/10.1016/0142-9612(87)90030-5.